Available online at www.sciencedirect.com
ScienceDirect
Spectrochimica Acta Part A 69 (2008) 41–48
SPECTROCHIMICA ACTA PART A
www.elsevier.com/locate/saa

Laser-diode-excited intense luminescence and green-upconversion in erbium-doped bismuth–germanate–lead glasses

G.F. Yang, Q.Y. Zhang *, T. Li, D.M. Shi, Z.H. Jiang

Key Laboratory of Specially Functional Materials of Ministry of Education and Institute of Optical Communication Materials, South China University of Technology, Guangzhou 510641, PR China

Received 4 November 2006; received in revised form 9 February 2007; accepted 9 March 2007

Abstract

We investigate the spectroscopic properties of the 1.5-μm emission from the $^4I_{13/2} \rightarrow {}^4I_{15/2}$ transition of Er^{3+} ions in bismuth–germanate–lead glasses for applications in broadband fiber amplifiers. The emission peak locates at 1532 nm with a full width at half-maximum (FWHM) of ~65 nm. The measured lifetime and the calculated emission cross-section of this transition are 3.3 ms and 8.66×10^{-21} cm^2, respectively. IR-to-green-upconversion occurs simultaneously upon excitation of the 1.5-μm emission with a commercially available 980 nm laser diode. Effects of PbF_2 content on the thermal stability, structure and spectroscopic properties of Er^{3+}-doped bismuth–germanate–lead glasses have been examined. We find that the substitution with PbF_2 provides a couple of potentials: shortening the UV cutoff band and decreasing the phonon energy of host glasses. Codoping of Yb^{3+} significantly enhances both the green-upconversion and 1.5-μm emission intensity by means of a nonradiative $Yb^{3+} \rightarrow Er^{3+}$ energy transfer. Energy transfer processes and nonradiative phonon-assisted decays could account for the population of the $^2H_{11/2}$ level, which is an emitting level of the green-upconversion of Er^{3+}. The results indicate the possibility towards the development of bismuth–germanate–lead based glasses as photonics devices.

Keywords: Glasses; Optical materials and properties; Er^{3+}; Upconversion; Raman spectra

1. Introduction

The optical properties of rare-earth (RE) doped solids have extensively been investigated over the last two decades [1]. However, the search for new materials with an improved functionality has still been an active area. In particular, the investigation of optimized glasses for broadband fiber amplifier, efficient lasing and frequency upconversion process requires more effort due to their potential applications [1]. Erbium ion (Er^{3+}) has been recognized as one of the most efficient RE ions for obtaining laser emission, frequency upconversion, and also in optical amplifiers and waveguide lasers, when doped in different hosts. Frequency upconversion in a variety of Er^{3+}-doped materials has been investigated in literature. Er^{3+}-doped glass fiber amplifier and waveguide laser, which are very attractive for their use in 1.5-μm optical telecommunication networks, which has also been demonstrated in silicate, phosphate and fluoride glasses [1,2].

Among the variety of existing glasses, heavy-metal oxide (HMO) glasses are becoming more interesting and attractive class of materials for photonics in recent years, because of their high refractive index and low cutoff phonon energy compared with other oxide glasses such as silicate or phosphate glasses [3–9]. In addition, a large amount of RE ions could be introduced in the HMO matrix and those could be used in the production of optical fibers and planar waveguides [3–9]. The reduced phonon energy increases the luminescence quantum yield from excited states of RE ions in these matrices and hence provides a possibility to develop more efficient lasers and fiber amplifiers at longer wavelengths compared to the other oxide glasses [3]. Bismuth–germanate–lead system has recently been investigated as a potential host for broadband fiber-optic amplifiers and all-solid-state upconversion lasers especially due to its their advantages such as the high refractive index, the low phonon energies, the good glass stability and chemical durability [3–9]. These special optical properties encourage in identifying them as important candidates for uses in photonic devices. In order to recognize the RE-doped-glass based photonic devices, the optical, mechanical, and thermal properties of the host materials could

* Corresponding author. Tel.: +86 20 87113681.
E-mail address: qyzhang@scut.edu.cn (Q.Y. Zhang).

1386-1425/$ – see front matter © 2007 Elsevier B.V. All rights reserved.
doi:10.1016/j.saa.2007.03.006

play a vital role and hence it has drawn our attention for consideration. In this paper, we present the development and a detailed experimental investigation on the thermal stability and spectroscopic properties of bismuth–germanate–lead glasses codoped with Er^{3+}/Yb^{3+}. In order to improve the optical properties, we partly replace the oxygen with fluorine, and specifically replacing PbO with PbF_2. Substitution with PbF_2 provides a couple of potentials: shortening the UV cutoff band and decreasing the phonon energy of host glasses. Effects of PbF_2 presence in the matrix on the structure and spectroscopic properties of Er^{3+}/Yb^{3+}-codoped bismuth–germanate–lead glasses have been investigated.

2. Experiment

Bismuth–germanate–lead glasses with molar composition of $25Bi_2O_3$–$62GeO_2$–$(13–x)$PbO–xPbF$_2$–yEr$_2$O$_3$ (BGPP1) ($x = 0$, 4, 8 and 13; $y = 0.25$, 0.5, 1, 1.5, and 2) for near-infrared emission and $25Bi_2O_3$–$62GeO_2$–$(13–x)$PbO–xPbF$_2$–Er$_2$O$_3$–yYb$_2$O$_3$ (BGPP2) ($x = 0$, 4, 8 and 13; $y = 1$, 2, and 5) for upconverted luminescence were prepared by melting 15 g batches with the reagent-grade chemicals of Bi_2O_3, GeO_2, PbO, PbF_2, Er_2O_3 and Yb_2O_3 in a platinum crucible for 20 min at 950–1000 °C. The melts were then quenched on preheated (180 °C) stainless steel blocks and annealed at a temperature close to the vitreous transition temperature for 2 h before ramping down to room temperature. After annealed, samples for optical and spectral properties measurements were cut into rectangular 5 mm × 4.5 mm × 1.2 mm shapes and optically polished.

The refractive index was measured on a Metricon 2010 by means of the prism coupling technique. A 0.8 mW He–Ne laser tube with standard silicon detectors was employed operating at 0.633 μm. The density of the sample was measured using Archimedes' liquid immersion method on an analytical balance. Glass transition and crystallization temperatures were measured on the powered samples using a Netzsch STA 449C Jupiter different scanning calorimeter (DSC) at a heating rate of 10 °C/min from room temperature (RT) to 700 °C. Raman spectra were measured on a visible Renishaw micro-Raman spectrometer, which was fitted with a 514.5 nm Ar^+ laser wavelength. A standard Olympus microscope objective s350d was used to focus the incident laser beam to a spot size of 2 μm onto the sample and scattered light was collected by a charge-coupled device detector array. The absorption spectra were obtained from a Perkin-Elmer LAMBDA 900 UV/Vis/NIR spectrophotometer from 400 to 2000 nm with a resolution of 1 nm. The fluorescence spectra were measured on a computer-controlled Triax 320 spectrofluorimeter (Jobin-Yvnon Inc.) upon excitation of a 980 nm LD. Emitted light was focused on to the monochromator and was monitored at the exit slit by a photon-counting R5108 photomultiplier tube (400–1200 nm) for the visible upconversion emission and InGaAs detector (800–1650 nm) for 1.5-μm emission. The temporal decay curves of the fluorescence signals for 1550 nm band of Er^{3+} were stored after averaging 128 times by a Tektronix TDS3012B digital phosphor oscilloscope. The lifetimes of $^4I_{13/2}$ levels were obtained by fitting the exponential function to the experimentally observed fluorescence decay curves.

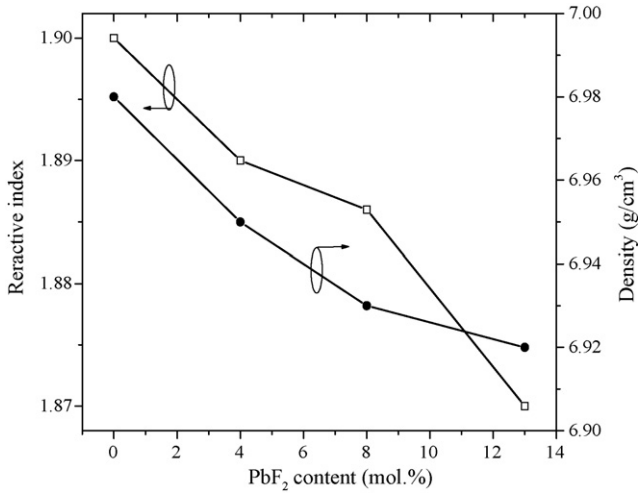

Fig. 1. The compositional-dependence of refractive indices and densities of BGPP1 glasses.

3. Results and discussion

3.1. Physical and thermal stability analysis

Fig. 1 shows the compositional-dependent refractive indices and glass densities of BGPP1 glasses. It is noted that with increasing the PbF_2 content, the refractive indices and densities of the BGPP1 glasses decrease quite significantly from 1.900 to 1.871, and 6.98 to 6.92, respectively, that might be due to the modifications in the structure of the glasses caused by the gradual replacement of the Pb=O double bonds with two Pb–F single bonds.

Table 1 presents the measured DSC data of BGPP1 and PbF_2 modified BGPP1 glasses. The difference between the glass tran-

Table 1
Physical and thermal properties of BGPP glasses

Glass	Composition (mol.%)				T_g (°C)	T_x (°C)	ΔT (°C)	n_d	ρ (g/cm^3)
	GeO_2	Bi_2O_3	PbO	PbF_2					
BGPP1									
$x = 0$	62	25	13	0	437	528	91	1.900	6.98
$x = 4$	62	25	9	4	425	512	87	1.889	6.95
$x = 8$	62	25	5	8	411	467	86	1.886	6.93
$x = 13$	62	25	0	13	401	485	84	1.871	6.92

sition temperature (T_g) and the onset crystallization temperature (T_x), $\Delta T = T_x - T_g$, has been frequently used as an approximate estimation of the glass formation ability or glass thermal stability. Larger the ΔT value stronger will be the inhibition in the process of nucleation and crystallization, and consequently the greater the glass-forming tendency. For a glass it is desirable to have larger ΔT value. The glass transition temperature and the onset crystallization temperature of the BGPP1 ($x = 0$) are 437 and 528 °C, respectively. Fiber could be made from this glass since ΔT is 91 °C, which is higher than that of fluorozirconate glasses. It is noted that the values of T_g's and T_x's decreased as the PbF_2 concentration is increased, as shown in Table 1. However, no significant change in ΔT's has been confirmed. Therefore, the PbF_2 substitution has very limited influence on the thermal stability in this BGPP glass system from the aspect of the difference ΔT.

3.2. Raman spectra

Raman spectra of BGPP1 and also PbF_2 modified BGPP1 glasses are shown in Fig. 2(a and b), respectively. The spectra contain three spectral regions: (1) low-frequency region $\leq 250\,cm^{-1}$, which is attributed to the collective modes of local structures and heavy metal vibrational modes, (2) intermediate region of 300–600 cm^{-1}, which is assigned to the deformation of vibrational modes of a glass network structure with bridged oxygen, and (3) high-frequency region $\geq 600\,cm^{-1}$, which is attributed to the stretching vibrational modes of the glass network former [5,7,9–11]. Deconvolution of Raman spectrum of BGPP1 in Fig. 2(a), strong 395, and 535 cm^{-1} vibrational modes along with a relatively weak 765 cm^{-1} band have been identified in spectral regions 300–600 cm^{-1}, and $\geq 600\,cm^{-1}$, are assigned to the vibrations of Bi–O–Pb and Ge–O–Pb bridges (395 cm^{-1} band); the stretching vibrations of Bi–O–Bi and Ge–O–Ge bridges (535 cm^{-1} band); and the stretching vibrations of $[GeO_4]^{2-}$ tetrahedra (765 cm^{-1} band), respectively. It is worthwhile to mention here that significant cure-shape changes have been observed in the glass samples with PbF_2 availability in the glass matrix. It is noticed that the Raman scattering from Ge–O stretching modes has slightly been shifted towards the lower frequency from 765 to 740 cm^{-1} with an increase of PbF_2 content up to 13 mol.%. Meanwhile, the 535 cm^{-1} bands intensity have slightly reduced and the 395 cm^{-1} band intensity has been increased, might be originated from the Pb–F vibrational bonds (~345 cm^{-1}). The incorporation of PbF_2 into BGPP glasses might also be resulting changes of the glass network due to depolymerization of the glass network by considering the values of electronegativity, for Pb, O and F elements, are 2.33, 3.44 and 3.98, respectively, the covalency of Pb–F bond is weaker than that of Pb–O bond, it is expected that the influence of the Pb–F bond on the local ligand environments around Er^{3+} decrease with an increase of PbF_2 content.

3.3. Absorption spectra and Judd–Ofelt analysis

Fig. 3 shows room temperature absorption spectra of Er^{3+}-doped BGPP1 glasses. The assignments of absorption band indicate the excited level. The inset in Fig. 3 illustrates the wavelength dependence of the transmittances of the BGPP1 glasses. It is noted that the wavelengths of the UV cutoff wavelength has been changed significantly with an increase in PbF_2 concentration. With an extrapolation to the zero transmittance at the steepest slope, the cutoff wavelengths for $x = 0$, 4, 8 and 13 were estimated to be 439, 428, 421, and 410 nm, respectively. It is desirable for a glass host to have as large UV transmittance as possible for laser and upconversion applications.

The Judd–Ofelt theory [12] has often been used to calculate the spectroscopic parameters, such as strength parameters, spontaneous emission probability, branching ratio, and radiation

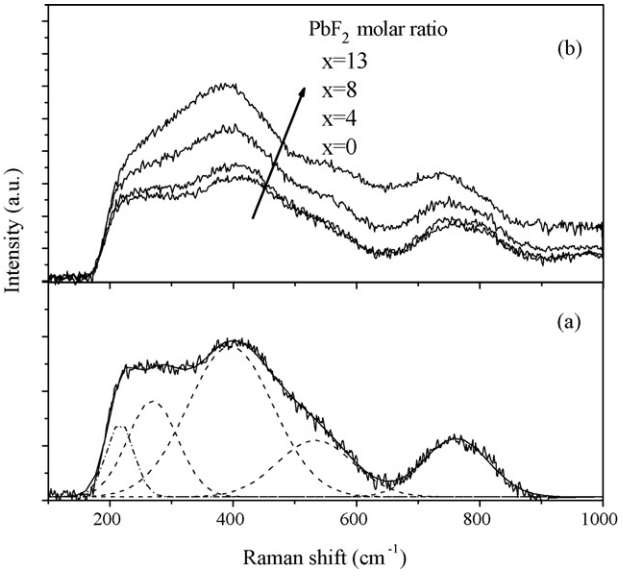

Fig. 2. Raman spectra of BGPP1 ($x = 0$) with fitting data (a) and PbF_2 modified BGPP1 (b). Curves were Y-shifted for clarity.

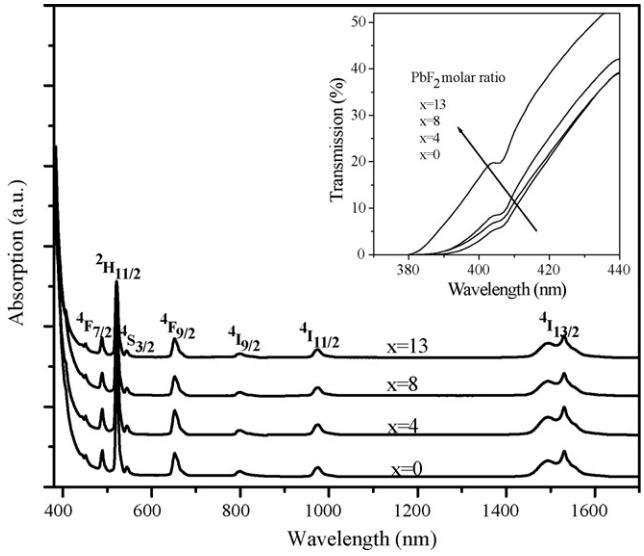

Fig. 3. Room temperature absorption spectra of Er^{3+}-doped BGPP1 ($y = 1$) glasses. The assignments of absorption band indicate the excited level. Inset shows the wavelength dependence of the transmittance of the PbF_2 modified BGPP1 glasses ($x = 0$, 4, 8 and 13).

lifetime, of rare earths in various matrixes. The three parameters Ω_t ($t=2,4,6$) can be obtained experimentally from the measured absorption spectrum and the refractive index of the host material [13,14]. For the transitions between the states which meet the transition selective rules $\Delta S=\Delta J=0$, $\Delta J=0, 1$, there exists the contribution of magnetic dipole transitions, S_{md}, which can be calculated by [15]:

$$S_{md}=\frac{1}{4m^2c^2}|\langle[S,L]J||L+2S||[S',L']\rangle J'|^2 \quad (1)$$

where m is mass of the electron, c the velocity of light, the $M=|\langle[S,L]J||L+2S||[S',L']J'\rangle|$ matrix elements between SLJ states are

- for $J'=J-1$,

$$M=\hbar\left\{[(S+L+1)^2-J^2]\frac{[J^2-(L-S)^2]}{4J}\right\}^{1/2} \quad (2)$$

- for $J'=J$,

$$M=\hbar\left[\frac{2J+1}{4J(J+1)}\right]^{1/2}[S(S+1)-L(L+1)+3J(J+1)] \quad (3)$$

- for $J'=J+1$,

$$M=\hbar\left\{[(S+L+1)^2-(J+1)^2]\frac{[(J+1)^2-(L-S)^2]}{4(J+1)}\right\}^{1/2} \quad (4)$$

where $\hbar=h/2\pi$, h is the Planck constant, J the total angular momentum, L the orbit angular momentum, and S is the total spin-orbin angular momentum. In the case of the $^4I_{13/2}\rightarrow{}^4I_{15/2}$ transition of Er^{3+}, the difference in the total angular momentum $\Delta J=1$. To obtain wide and flat 1.55-μm emission spectra, it is effective to increase the relative contribution of the electric-dipole transition (S_{ed}) [16]. The S_{md} is independent of ligand fields and is characteristic to the transition determined by the quantum numbers, while that of the S_{ed} is a function of the ligand fields. And it is possible to increase the fraction of the electric-dipole transition by modifying the composition and structures of the hosts. According to the Judd–Ofelt theory, the S_{ed} of $^4I_{13/2}\rightarrow{}^4I_{15/2}$ transition of Er^{3+} is given by: $S_{ed}[^4I_{13/2}, {}^4I_{15/2}]=0.0188\,\Omega_2+0.1176\,\Omega_4+1.4617\,\Omega_6$ [17], where the three coefficients Ω_ts are the reduced matrix elements of the unit tensor operators provided in Refs. [17,18], and coefficients Ω_t ($t=2, 4, 6$) are the intensity parameters. Table 2 shows comparisons of the Judd–Ofelt intensity parameters, Ω_t ($t=2$, 4, 6), of Er^{3+} in various glass hosts. According to previous studies [16], Ω_2 is related with the symmetry of the glass hosts while Ω_6 is inversely proportional to the covalency of Er–O bond. The Er–O bond is assumed to be dependent on the local basicity around the rare-earth sites, which can be adjusted by the composition or structure of the glass hosts. The Ω_2 values of BGPP1 glasses are larger than those of other glasses due to the fact of large polarization of the Ge^{4+} and the asymmetric of BGPP1. It should be mentioned here that the Ω_6 values in BGPP are comparable to those of fluoride glasses [19] and are larger than those in silicate, aluminate, germanate and tellurite glasses [19]. As shown in Table 2, with increasing PbF_2 content, the value of Ω_2 decreases monotonically from 4.93 to 3.63, meanwhile the value of Ω_6 slightly decreases from 1.04 to 0.86, indicating the influence of the Pb–F bond on the local ligand environments around Er^{3+} decrease with an increase of PbF_2 content, consequently, the covalency of the Er–O bond increases, and the value of Ω_6 decrease accordingly. Table 3 represents the calculated results of the electric-dipole transition rates, A_{ed}, and magnetic-dipole transition rates, A_{md}, total radiative rates, A_r, and radiative lifetimes, τ_{rad}, of the $^4I_{13/2}$ level of Er^{3+}-doped BGPP glasses, where the A_r can be calculated by [20]:

Table 2
Judd–Ofelt intensity parameters of Er^{3+} in various glass hosts

Glasses	Ω_2 (10^{-20} cm^2)	Ω_4 (10^{-20} cm^2)	Ω_6 (10^{-20} cm^2)
BGPP1			
$x=0$	4.96	1.29	1.08
$x=4$	4.93	1.66	1.04
$x=8$	3.85	1.35	0.93
$x=13$	3.63	1.84	0.86
Tellurite [18]	4.12	1.81	0.85
Silicate [19]	4.23	1.04	0.61
Phosphate [19]	6.65	1.52	1.11
Aluminate [19]	5.60	1.60	0.61
Germanate [19]	5.81	0.85	0.28
Fluoride [19]	2.91	1.27	1.11

$$A_r=A_{ed}+A_{md}=\frac{64\pi^4e^2}{3h\lambda_m^3(2J+1)}\times\left[\frac{n(n^2+2)^2}{9}S_{ed}+n^3S_{md}\right] \quad (5)$$

where e is the elementary charge and n is the refractive index at the mean wavelength, λ_m. It is found that BGPP1 glasses exhibit the large radiative transition probability (>200 s^{-1}) for the $^4I_{13/2}$ level of Er^{3+}, which is much larger than that in silicate and phosphate glasses, due to the higher J–O parameters and refractive index, indicates an enhanced local field and a larger radiative transition rate of Er^{3+} in the BGPP1 glasses.

Fig. 4 shows the absorption cross-section and stimulated emission cross-section of Er^{3+} for the 1.5-μm transition in BGPP1 ($x=0$) glass. The absorption cross-section has been

Table 3
The calculated electric-dipole transition rates, A_{ed}, magnetic-dipole transition rates, A_{md}, total radiative rates, A_r, and radiative lifetimes, τ_{rad}, of the $^4I_{13/2}$ level of Er^{3+}-doped BGPP1 glasses

x (mol.%)	A_{ed} (s^{-1})	A_{md} (s^{-1})	A_r (s^{-1})	τ_{rad} (ms)	τ_m (ms)	η (%)
0	175	70	245	4.09	3.3	80.7
4	139	70	239	4.28	4.0	93.4
8	134	70	204	4.91	4.5	91.6
13	134	68	202	4.96	4.8	96.8

Table 4
Comparisons of FWHM, σ_{emi}, τ_m, FWHM × σ_{emi} and $\sigma_{emi} \times \sigma_m$ of Er^{3+} in different glass hosts

Glasses	σ_{emi} ($\times 10^{-21}$ cm^2)	FWHM (nm)	FWHM × σ_{emi}	τ_m (ms)	$\sigma_{emi} \times \tau_m$
BGPP1	7.04–8.66	62.2–64.5	443–559	3.3–4.8	28.5–38.1
Silicate [19]	5.5	40	220	–	–
Phosphate [19]	6.4	37	236.8	–	–
Bismuth [22]	7.0	79	554	1.9	13.3
Tellurite [22]	6.6	60	396	4.0	26.4
ZBLAN [22]	4.8	65	312	10	48

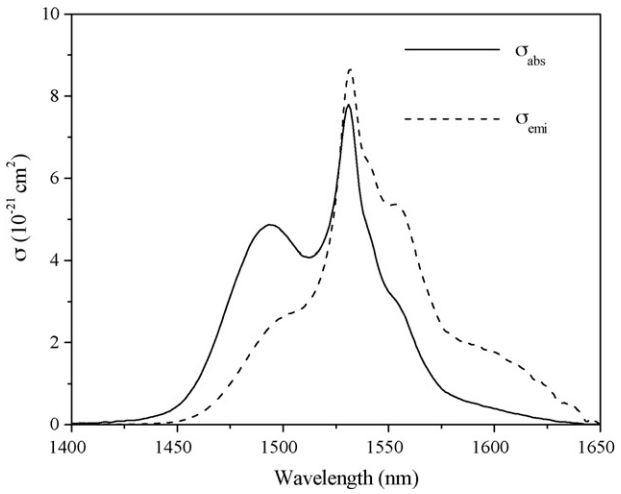

Fig. 4. Absorption and stimulated emission cross-sections of Er^{3+}-doped BGPP1 ($x=0$, $y=1$) glass.

determined from the absorption spectra, and the stimulated emission cross-section, σ_{emi}, has been calculated from McCumber method [21] by $\sigma_{emi}(\lambda) = \sigma_a(\lambda) \exp[(\varepsilon - h\gamma)/kT]$, where h is the Planck constant, k the Boltzmann constant, and ε is the net free energy required to excite one Er^{3+} from the $^4I_{15/2}$ state to $^4I_{13/2}$ state at temperature T. The stimulated emission cross-section for the $^4I_{13/2} \rightarrow {}^4I_{15/2}$ transition of Er^{3+} in different types of glass hosts is compared in Table 4. Since the stimulated emission cross-section is proportional to the host glass refractive index, $\sigma_{emi} \sim (n^2+2)^2/n$, it is apparent that Er^{3+} in BGPP1 glasses are capable of providing large stimulated emission cross-section at 1.5-μm bands. At this work, the σ^P_{emi} of the Er^{3+}-doped BGPP1 ($x=0$) is 8.66×10^{-21} cm^2, which is much higher than those of the silicate [19], phosphate [19], bismuth, tellurite [22] and fluoroziconate [22] glasses. With the substitution of PbO by PbF_2, σ_{emi} decreases monotonically from 8.66×10^{-21} to 7.04×10^{-21} cm^2, mainly due to the decrease in the refractive index values of the BGPP glasses.

3.4. Fluorescence spectra and lifetime

Fig. 5 illustrates the emission spectra of Er^{3+} in BGPP1 glasses. The broad 1.53-μm emission is assigned to the $^4I_{13/2} \rightarrow {}^4I_{15/2}$ transition, with a full width at half-maximum (FWHM) of ~65 nm. The Er^{3+} emission spectra in BGPP1 glasses are significantly broader compared with the other glasses studied as potential Er^{3+}-doped fiber amplifier (EDFA) hosts. It is noted that the FWHM increases with an increase in the Er^{3+} concentration as shown in Fig. 5(a). And, with the substitution of PbO by PbF_2 up to 13 mol.%, the FWHM slightly decreases from 64.5 to 62.5 nm, seen in Fig. 5(b). The dependence of the FWHM

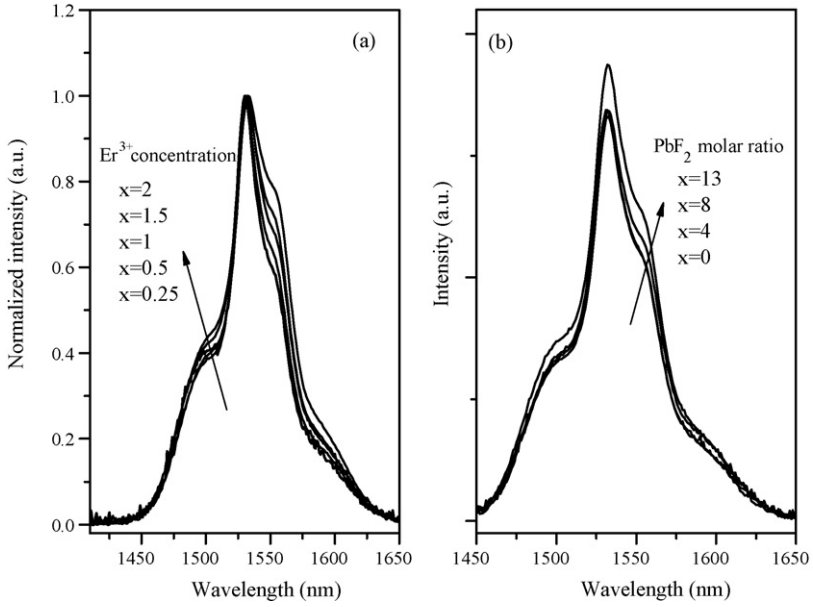

Fig. 5. 1.5-μm emission spectra of Er^{3+}-doped BGPP1 ($x=0$) (a), and PbF_2 modified BGPP1 ($y=1$) glasses (b).

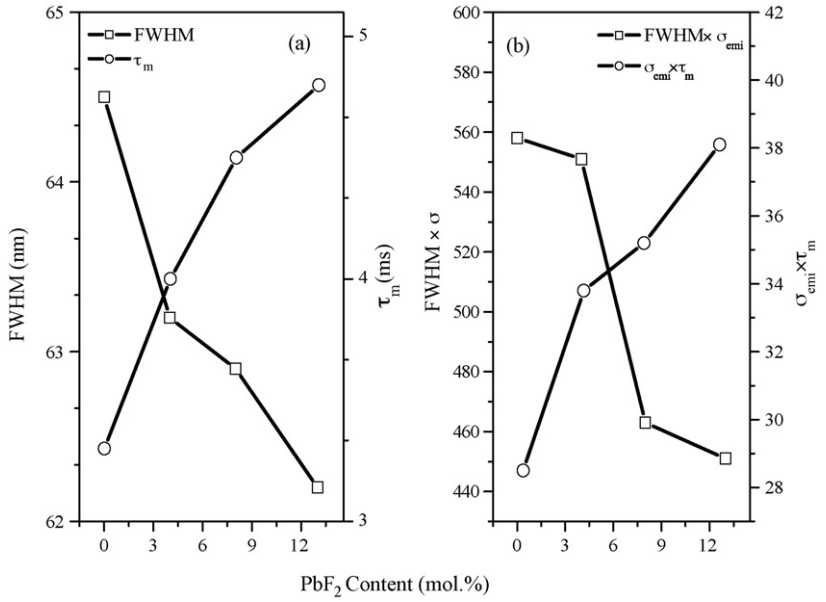

Fig. 6. Dependence of the FWHM and lifetime upon the PbF_2 concentration of Er^{3+}-doped BGPP1 (a), and dependence of the FWHM × σ_{emi} and $\sigma_{emi} \times \tau_m$ upon the PbF_2 concentration of Er^{3+}-doped BGPP1 (b).

and lifetime upon the PbF_2 concentration is shown in Fig. 6(a). It has clearly been seen that the lifetimes have increased almost linearly from 3.3 to 4.8 ms with an increase of PbF_2 concentration. Based on the J–O theory, the lifetime of the $^4I_{13/2}$ level is inversely proportional to the refractive index of glass. With the substitution of PbO by PbF_2, the decrease of the refractive index leads to an increase of the lifetime of the $^4I_{13/2}$ level. The compositional-dependent lifetime and the quantum efficiency of the $^4I_{13/2}$ level are also summarized in Table 3. Obviously, quantum efficiency has increased quite significantly from 80.7 to 96.8% with an increase in PbF_2 concentration, which might be due to a decrease in the phonon energy of the BGPP1 glasses as shown in Fig. 2, and the reduced OH^- groups content with the substitution of PbF_2 for PbO.

The gain bandwidth of an amplifier is determined largely by the width of the emission spectrum and the stimulated emission cross-section. A figure-of merit (FOM) for bandwidth as the product FWHM × σ_e [9,19,22,23] along with the figure-of merit for amplifier gain $\sigma_{emi} \times \tau_m$ are listed in Table 4. Both the FWHM × σ_e product and the lifetime of the $^4I_{13/2}$ level are critical quality parameters for EDFA. Larger values of the FWHM × σ_e product and the longer lifetime imply wider gain bandwidth and lower pump threshold power [19,22]. The calculated values of the FWHM × σ_e product and the measured lifetime of the BGPP glass ($x = 0$) studied are 560 and 3.3 ± 0.2 ms, respectively. The dependence of the FWHM × σ_{emi} and $\sigma_{emi} \times \tau_m$ upon the PbF_2 concentration is shown in Fig. 6(b). It was clearly seen that the FWHM × σ_{emi} decrease from 560 to 450, meanwhile, $\sigma_{emi} \times \tau_m$ increase from 29 to 38 ms with increasing PbF_2 concentration. It should be mentioned here that the values of FWHM × σ_e of the BGPP1 glass studied are much higher than those of the fluoroziconate, silicate and phosphate glasses and are comparable with the tellurite glass. Figs. 4–6 clearly show that the apparent advantages of choosing BGPP1 glass hosts for designing broadband amplifiers.

3.5. Upconversion spectroscopy

The recorded room temperature upconversion fluorescence spectra of Er^{3+}/Yb^{3+}-dodoped GBPP2 glasses upon excitation of a 500 mW 980 nm LD have been shown in Fig. 7. The upconversion fluorescence at approximately 529, 545 and 657 nm, are assigned to the $^2H_{11/2} \rightarrow {}^4I_{15/2}$, $^4S_{3/2} \rightarrow {}^4H_{15/2}$, and $^4F_{9/2} \rightarrow {}^4H_{15/2}$ transitions of Er^{3+} ions, respectively. It is important to note that very strong green- and red-upconversion emissions at 545 and 657 nm have been observed in the visible spectrum. This result indicates that lasing could be expected from either the green or the red transitions with a suitable choice of cavity mirrors. Moreover, the result is in agreement with the predictions of the Judd–Ofelt theory since the branching ratios of the $^2H_{11/2} \rightarrow {}^4I_{15/2}$, and $^4F_{9/2} \rightarrow {}^4I_{15/2}$ transitions are 0.672 and 0.905, respectively. It is noted that both the green-upconversion intensity and the ratio between the intensities of red and green emissions increases very swiftly with the addition of Yb^{3+}, as shown in Fig. 7(a). The advent of highly Yb^{3+}-doped materials allowed a noticeable improvement in the upconversion efficiency in rare-earth doped glasses sensitized by ytterbium. When the GBPP2 glass is excited at 980 nm LD, an intense green-upconversion has been noticed by the naked eye, as shown in the inset in Fig. 7(b). Obvious increase in the intensity of the green-upconversion emissions due to an increase in PbF_2 content has also been clearly observed, as shown in Fig. 7(b). The significant increases of the intensity of the green-upconversion emissions with increase in PbF_2 content might be due to their lower phonon energy of the PbF_2 modified BGPP glasses as aforementioned in Fig. 2, which reduce nonradiative losses due to mutliphonon relaxation process, and also the reduced OH^- groups content with the substitution of PbF_2 for PbO.

The dependence of the visible fluorescence intensities upon excitation intensity has been examined and the results obtained from BGPP2 ($x = 0$, $y = 1$) are presented in log–log plot of

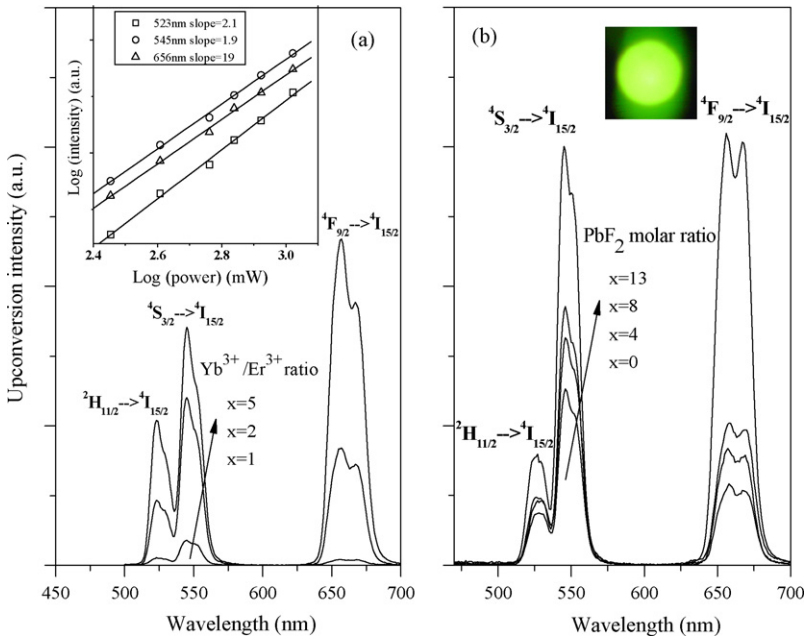

Fig. 7. Upconversion emission spectra of Er^{3+}/Yb^{3+}-codoped BGPP2 glasses under 980 nm LD excitation in (a) BGPP2 ($x=0$, $y=1$, 2, and 5), and (b) PbF_2 modified BGPP2 ($x=0$, 4, 8, and 13, $y=2$). The inset in (a) shows the dependence of the upconverted luminescence intensity upon the laser excitation intensity ($x=0$, $y=1$), and the inset in (b) is an optical image showing the green-upconversion emission for BGPP2 ($x=0$, $y=1$).

the inset figure of Fig. 7(a). It has been observed that the green emission at 529 and 545 nm signals could show approximately quadratic power law behaviors upon the pump intensity with the obtained slopes of 2.1 and 1.9, respectively, indicating two-photon processes [22,24]. Meanwhile, the dependence of the 657 nm upconverted fluorescence on pump power has also been found to be quadratic, the slope value obtained is 1.9, thereby indicating a two-photon process. Based on these spectroscopic measurements the following upconversion excitation mechanisms are proposed to be involved in the population of the relevant excited-state emitting levels of the Er^{3+}/Yb^{3+}-codoped glass, as shown in Fig. 8: (1) Er^{3+} ion is firstly excited initially from the ground state $^4I_{15/2}$ to the excited state $^4I_{11/2}$ through one of the following three processes under 980 nm excitation. (I) Ground-state absorption (GSA): $^4I_{15/2}$ (Er^{3+}) + a photon → $^4I_{11/2}$ (Er^{3+}), (II) phonon-assisted energy transfer (PAET) from the Yb^{3+} $^2F_{5/2}$ state: $^2F_{5/2}$ (Yb^{3+}) + $^4I_{15/2}$ (Er^{3+}) → $^2F_{7/2}$ (Yb^{3+}) + $^2I_{11/2}$ (Er^{3+}), and (III) ET from the $^2I_{11/2}$ state of adjacent Er^{3+}. Among the aforementioned three processes, PAET from Yb^{3+} is the dominant one, due to the larger absorption cross-section of Yb^{3+} at around 980 nm. (2) The ions at the populated $^4I_{11/2}$ state are promoted to the $^4F_{7/2}$ state by one of the following three processes. (I) Excited-state absorption (ESA): $^4I_{11/2}$ (Er^{3+}) + a photon → $^4F_{7/2}$ (Er^{3+}), (II) PAET from Yb^{3+}: $^2F_{5/2}$ (Yb^{3+}) + $^4I_{11/2}$ (Er^{3+}) → $^4F_{7/2}$ (Yb^{3+}) + $^4F_{7/2}$ (Er^{3+}), and (III) ET from the $^4I_{11/2}$ state of adjacent Er^{3+}: $^4I_{11/2} + {}^4I_{11/2} \rightarrow {}^4F_{7/2} + {}^4I_{15/2}$. Er^{3+} ions at the populated $^4F_{7/2}$ state can relaxes nonradiative relaxation (NR) very fast to the intermediate state of $^2H_{11/2}$ due to a multiphonon relaxation process (MRP), the $^2H_{11/2} \rightarrow {}^4I_{15/2}$ transition shows the 529 nm green emission. Er^{3+} ion at the $^4F_{7/2}$ state can also decay rapidly down to the $^4S_{3/2}$ state, and finally, the $^4S_{3/2} \rightarrow {}^4I_{15/2}$ transition reveals an intense green-upconversion at 545 nm. For the red-upconversion emission at 657 nm, Er^{3+} ion is first excited from the ground state $^4I_{15/2}$ to the excited $^4I_{11/2}$ through the aforementioned three processes: GSA, PAET and ET under 980 nm excitation. The Er^{3+} ions populated $^4I_{11/2}$ state then decays NR to the long-living $^4I_{13/2}$ state due to MRP, and are promoted to the $^4F_{9/2}$ state by one of the following processes. (I) ESA: $^4I_{13/2}$ (Er^{3+}) + a photon → $^2F_{9/2}$ (Er^{3+}), (II) PAET from Yb^{3+}: $^2F_{5/2}$ (Yb^{3+}) + $^4I_{13/2}$ (Er^{3+}) → $^2F_{7/2}$ (Yb^{3+}) + $^4F_{9/2}$ (Er^{3+}), and (III) ET from the $^4I_{11/2}$ state of adjacent Er^{3+}:

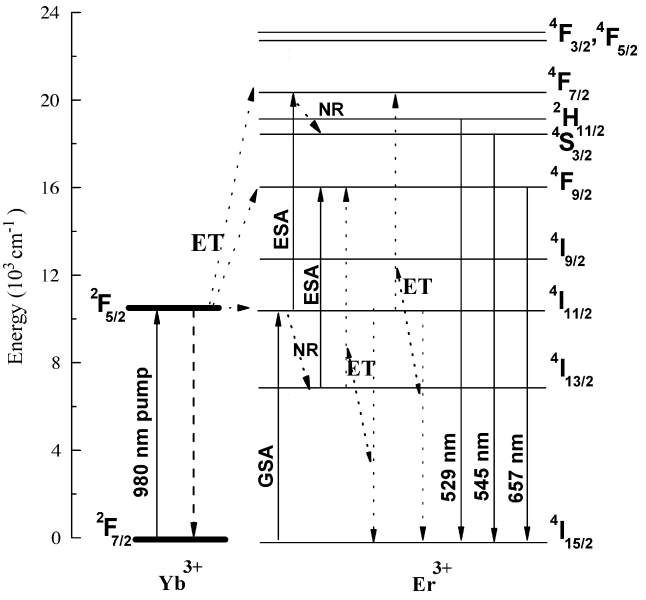

Fig. 8. Schematic energy level diagram of Er^{3+}/Yb^{3+}-doped BGPP2 glasses. The possible upconversion emission mechanism is indicated.

$^4I_{11/2} + {}^4I_{13/2} \rightarrow {}^4I_{15/2} + {}^4F_{9/2}$, and also (IV) a contribution from higher-energy state $^4S_{3/2}$ through a nonradiative relaxation, and finally, the $^4F_{9/2} \rightarrow {}^4I_{15/2}$ transition gives 657 nm red emission. It should be mentioned here that the red-emission in the PbF_2 modified BGPP are also found to be as intense as that of the green emission at 545 nm, which might be due to the high PAET from Yb^{3+} to Er^{3+}, and the high ET from the $^4I_{13/2}$ state. The ratio between the intensities of red and green emissions increases very swiftly from 0.58 to 1.32 with an increase in the PbF_2 content up to 13 mol.%. The populations of the $^4F_{9/2}$ state compared to that of $^4S_{3/2}$ state in the PbF_2 modified BGPP being caused due to the addition of fluorine, which increases the mass of the ligands resulting the reduction of phonon vibration energies and thus a reduction in the MRP rate.

Based on their 1.5-μm radiative emission and upconversion performance from infrared to green as has been discussed and explained here, we conclude these BGPP and PbF_2 modified BGPP doped with Er^{3+} and codoped with Er^{3+}/Yb^{3+} could be suggested as more promising and quite useful optical materials towards the development of optical amplifier and upconversion laser glass materials, respectively.

4. Conclusion

In summary, we report on the experimental investigation of thermal stability and spectroscopic properties of Er^{3+}- and/or Er^{3+}/Yb^{3+}-doped BGPP and PbF_2 modified BGPP glasses. Broadband 1.5-μm emission with the measured peak wavelength of 1532 nm and FWHM of ∼65 nm has been obtained in Er^{3+}-doped BGPP glass upon excitation with a conventional 980 nm LD. Intense room temperature green-upconversion has also been observed in Er^{3+}/Yb^{3+}-codoped BGPP glasses and the involved mechanism has been explained. The addition of PbF_2 leads to the reduction of the UV cutoff band and also the reduction of phonon energy in the host glasses. The broadband 1.5-μm emission of Er^{3+}-doped samples and the strong green-upconversion of Er^{3+}/Yb^{3+}-codoped samples and their high thermal stability have demonstrated a strong and promising potentiality towards the development of an oxide-based fiber amplifier and green-upconversion glass-fiber laser, respectively.

Acknowledgments

The authors acknowledge financial support from NSFC (50472053), NCET (04-0823), DSTG (04020036, 2004A10602002 and 2006J1-C0491).

References

[1] M.J.F. Digonnet, Rare-Earth-Doped Fiber Lasers and Amplifiers, Marcel Dekker, New York, 2001, p. 1.
[2] R. Reisfeld, C.K. Jorgensen, Lasers and Excitated states of Rare-earth, Springer, New York, 1977, p. 1.
[3] R. Balda, J. Fernandez, M. Sanz, A. de Pablos, J. Mugnier, Phys. Rev. B 61 (2000) 3384.
[4] H. Takebe, K. Yoshino, T. Murata, K. Morinaga, D.W. Hewak, J. Wang, D.N. Payne, Appl. Opt. 36 (1997) 5839.
[5] A.E. Miller, K. Nassau, K.B. Lyons, M.E. Lines, J. Non-Cryst. Solids 99 (1988) 289.
[6] C.B. Layne, W.H. Lowdermilk, M.J. Weber, Phys. Rev. B 16 (1977) 10.
[7] Q.Y. Zhang, T. Li, Z.H. Jiang, Appl. Phys. Lett. 87 (2005) 171911.
[8] Q.Y. Zhang, T. Li, D.M. Shi, G.F. Yang, J. Appl. Phys. 99 (2006) 033510.
[9] D.D. Chen, Y.H. Liu, Y.F. Zhou, Mater. Chem. Phys. 90 (2005) 78.
[10] L. Baia, R. Stefan, E. Popp, S. Simon, W. Kiefer, J. Non-Cryst. Solids 324 (2003) 109.
[11] Z.D. Pan, S.H. Morgan, K. Dyer, A. Ueda, J. Appl. Phys. 79 (1996) 8906.
[12] (a) B.R. Judd, Phys. Rev. 127 (1962) 750;
(b) G.S. Ofelt, J. Chem. Phys. 37 (1962) 511.
[13] S. Tanabe, T. Ohyagi, N. Soga, T. Hanada, Phys. Rev. B 46 (1992) 3305.
[14] H. Takebe, Y. Nageno, K. Morinaga, J. Am. Ceram. Soc. 78 (1995) 1161.
[15] S. Tanabe, J. Non-Cryst. Solids 259 (1999) 1.
[16] W.T. Lirnall, P.R. Fields, B.G. Wybourne, J. Chem. Phys. 42 (1965) 3797.
[17] M.J. Weber, Phys. Rev. 157 (1967) 262.
[18] Y. Ohishi, A. Mori, M.Y. Yamada, Opt. Lett. 23 (1998) 274.
[19] X. Zou, T. Izumitani, J. Non-Cryst. Solids 162 (1993) 68.
[20] R.R. Jacobs, M.J. Weber, IEEE J. Quantum Electron. QE-12 (1976) 102.
[21] D.E. McCumber, Phys. Rev. 134 (1964) A299.
[22] S. Shen, M. Naftaly, A. Jha, Proc. SPIE 3849 (1999) 103.
[23] J.H. Yang, The study of luminescent properties of Er^{3+} doped (halide) tellurite and bismuth-based glasses, Ph.D. Thesis, Shanghai Institute of Optical and Fine Mechanics, Chinese Academy of Science, Shanghai, China, 2004.
[24] M. Pollnau, D.R. Gamelin, Phys. Rev. B 61 (2000) 3337.